Human Molecular Genetics, 2013, Vol. 22, No. 13 **2662–2675**
doi:10.1093/hmg/ddt115
Advance Access published on March 7, 2013

Heterochromatinization induced by GAA-repeat hyperexpansion in Friedreich's ataxia can be reduced upon HDAC inhibition by vitamin B3

Ping K. Chan[1,†], Raul Torres[1,†], Cihangir Yandim[1], Pui P. Law[1], Sanjay Khadayate[2], Marta Mauri[1], Crina Grosan[3], Nadine Chapman-Rothe[1], Paola Giunti[5], Mark Pook[4] and Richard Festenstein[1,*]

[1]Gene Control Mechanisms and Disease Group, MRC Clinical Sciences Centre, Imperial College School Medicine, [2]Genes and Metabolism Section, MRC Clinical Sciences Centre, Hammersmith Hospital Campus. Du Cane Road, London W12 0NN, UK, [3]Information Systems and Computing, [4]Hereditary Ataxia Group, Centre for Cell & Chromosome Biology and Brunel Institute of Cancer Genetics & Pharmacogenomics, Division of Biosciences, School of Health Sciences & Social Care, Brunel University, Uxbridge UB8 3PH, UK and [5]Institute of Neurology, University College London, Queen Square, London

Received February 5, 2013; Revised February 5, 2013; Accepted March 3, 2013

Large intronic expansions of the triplet-repeat sequence (GAA.TTC) cause transcriptional repression of the Frataxin gene (*FXN*) leading to Friedreich's ataxia (FRDA). We previously found that GAA-triplet expansions stimulate heterochromatinization *in vivo* in transgenic mice. We report here using chromosome conformation capture (3C) coupled with high-throughput sequencing that the GAA-repeat expansion in FRDA cells stimulates a higher-order structure as a fragment containing the GAA-repeat expansion showed an increased interaction frequency with genomic regions along the *FXN* locus. This is consistent with a more compacted chromatin and coincided with an increase in both constitutive H3K9me3 and facultative H3K27me3 heterochromatic marks in FRDA. Consistent with this, DNase I accessibility in regions flanking the GAA repeats in patients was decreased compared with healthy controls. Strikingly, this effect could be antagonized with the class III histone deactylase (HDAC) inhibitor vitamin B3 (nicotinamide) which activated the silenced *FXN* gene in several FRDA models. Examination of the *FXN* locus revealed a reduction of H3K9me3 and H3K27me3, an increased accessibility to DNase I and an induction of euchromatic H3 and H4 histone acetylations upon nicotinamide treatment. In addition, transcriptomic analysis of nicotinamide treated and untreated FRDA primary lymphocytes revealed that the expression of 67% of genes known to be dysregulated in FRDA was ameliorated by the treatment. These findings show that nictotinamide can up-regulate the *FXN* gene and reveal a potential mechanism of action for nicotinamide in reactivating the epigenetically silenced *FXN* gene and therefore support the further assessment of HDAC inhibitors (HDACi's) in FRDA and diseases caused by a similar mechanism.

INTRODUCTION

Friedreich's ataxia (FRDA), an autosomal recessive neurodegenerative disease, is the commonest form of hereditary ataxia. It is caused by abnormal expansion of a DNA triplet-repeat (GAA) sequence located within intron 1 of the *FXN* gene. FRDA patients carrying GAA.TTC repeats, with expansions ranging from 66 to 1700 or even more, have reduced levels of Frataxin mRNA and protein (1). Frataxin is a conserved mitochondrial protein which has multiple functions including chaperoning iron during iron–sulfur cluster

*To whom correspondence should be addressed. Tel: +44 2083838310; Fax: +44 2083838306; Email: r.festenstein@imperial.ac.uk
†These authors contributed equally to this work.

biogenesis, control of iron-mediated oxidative tissue damage and heme biosynthesis (2). Reduced levels of Frataxin results in mitochondrial dysfunction and pathology, affecting mainly the dorsal root ganglia, sensory nerves, corticospinal tracts and dentate nuclei (3). The size of the GAA-repeat expansion in FRDA correlates with disease severity and inversely with the age of onset (4). Patients with an onset in childhood usually have longer GAA expansions and the characteristic symptoms consist of dis-coordination, slurred speech, peripheral neuropathy and cardiomyopathy (5,6). At present no effective treatment is available for FRDA, severe disability generally occurs by early adulthood and severely affected individuals can die from cardiomyopathy.

A number of molecular models have been proposed to explain the transcriptional silencing of *FXN* triggered by the intronic GAA expansion. Bidichandani *et al*. had first suggested that GAA repeats form an unusual DNA–RNA hybrid structure, which impedes the progress of RNA polymerase II, resulting in silencing of the gene (7–9). More recently, we established that GAA repeats can induce heterochromatin-mediated gene silencing in a transgenic mouse model (10). These *in vivo* data showed that triplet-repeat sequences could induce the formation and/or maintenance of heterochromatinization; thus, inhibition of access of transcription factors to the gene could be one of the mechanisms underlying *FXN* gene silencing (11). Furthermore, modifications associated with a high-order chromatin structure, i.e. hypoacetylation of histones H3 and H4 and hypermethylation of lysine 9 in histone H3 (H3K9me2 and H3K9me3) have been found in the immediate vicinity of the GAA-repeat expansion in both the FRDA lymphoblastoid cell line and primary lymphocyte models, and also in FRDA human and transgenic mouse tissues (4,12–14). All these data support the notion that this repeat sequence can induce heterochromatinization spreading into the regions flanking the GAA repeat in FRDA-affected individuals (4,11).

The decision to activate or silence a gene depends on the balance between positively acting factors generally contributed by acetylation marks on the core histones, and negative factors such as K9 and K27 trimethylation of histone H3, which promote the formation of a condensed higher–order chromatin structure (15). This regular higher-order structure is thought to reduce the accessibility of the transcriptional machinery, resulting in transcriptional silencing of the affected gene. On the basis of this theory, *in vivo* and *in vitro* FRDA models have been treated with histone deactylase inhibitors (HDACi's) by different research groups and the silenced *FXN* gene was reactivated to various levels (12,16–19). In recent years, HDAC inhibition has been found to be potentially valuable in cancer treatment as it has been shown to induce selective apoptosis in tumor cells, and some HDACi's have progressed to clinical trials (20,21). Previous studies using FRDA patient cell lines and transgenic mouse models suggested that several common and highly active HDACi's targeting Class I & II HDACs, such as sodium valproate (22), trichostatin A (12), suberoylanilide hydroxamic acid (12) and suberoyl bishydroxamic acid (17), had no significant effect on *FXN* gene expression. A commercially available Class I HDACi (BML-210) was first found to up-regulate *FXN* mRNA expression in 2006 (12). Subsequent synthesis of derivatives of this benzamide identified a series of pimelic o-aminobenzamide compounds, all of which preferentially inhibit Class I HDACs, have been shown to reverse silencing of *FXN* in various FRDA models to differing extent (17–19). Although these compounds can restore *FXN* expression, none of them have been licensed for use in humans. We therefore focused our efforts on a ready-to-use HDACi, nicotinamide, and investigated whether it could be used to reverse the silencing of the *FXN* gene in FRDA.

Nicotinamide is a precursor of nicotinic acid and a form of vitamin B which was shown to be potentially useful for treating mitochondrial encephalopathies and neurodegenerative diseases (23). Biochemically, nicotinamide acts as a non-competitive end product inhibitor of the NAD^+-dependent histone deacetylase Sir2 family (24). In humans, among the seven identified Sir2 homologs (SIRT1-7), only SIRT1 is predominantly localized to the nucleus. In both *in vitro* and mammalian cell models, nicotinamide has been found to effectively inhibit the enzymatic activity of SIRT1 which plays a critical role in the formation of repressive heterochromatin by different mechanisms including deacetylation of histone tails (25), recruitment of deacetylated histone H1 (26) and regulation of histone methyltransferase (SUV39-H1) activity (27).

Previous epigenetic studies have provided evidence of the GAA expansion-induced transcriptional inhibition in FRDA, and linked this to changes in histone modifications (4,12–14). However, no studies have focused directly on elucidating the higher-order chromatin structure. Therefore, we first set out to investigate the heterochromatic structure of the *FXN* gene locus by using the chromosome conformation capture technique coupled with high-throughput sequencing (3C-seq) (28,29), DNase I accessibility assays (30) as well as chromatin immunoprecipitation (ChIP) (31). Our data suggest that a high order of chromatin organization at exon 1 of the *FXN* locus might be responsible for the transcriptional silencing seen in FRDA. We then went on to show that nicotinamide can increase *FXN* mRNA expression in several FRDA models, i.e. Epstein barr virus (EBV)-transformed cell lines, human primary cultured lymphocytes and transgenic mice. Furthermore, epigenetic changes caused by nicotinamide treatment, including the reduction of heterochromatic H3K9me3 and H3K27me3 together with the induction of euchromatic H3 and H4 histone acetylation, strongly suggest that it can reactivate *FXN* transcription by reversing the condensed chromatin structure induced by GAA-repeat expansion. Interestingly, alongside the increased *FXN* expression with nicotinamide treatment, expression of a subset of genes known to be dysregulated in FRDA was corrected (32). From a therapeutic point of view, nicotinamide is a potential candidate drug for FRDA treatment as it has been used in various therapeutic applications over the past 40 years and has a good safety profile (33). Our data provide valuable information to promote the development of a potential radical therapy for FRDA which has no effective cure at present. However, it should be stressed that further assessment of the safety and tolerability of nicotinamide need to be done before it can be given to patients with FRDA.

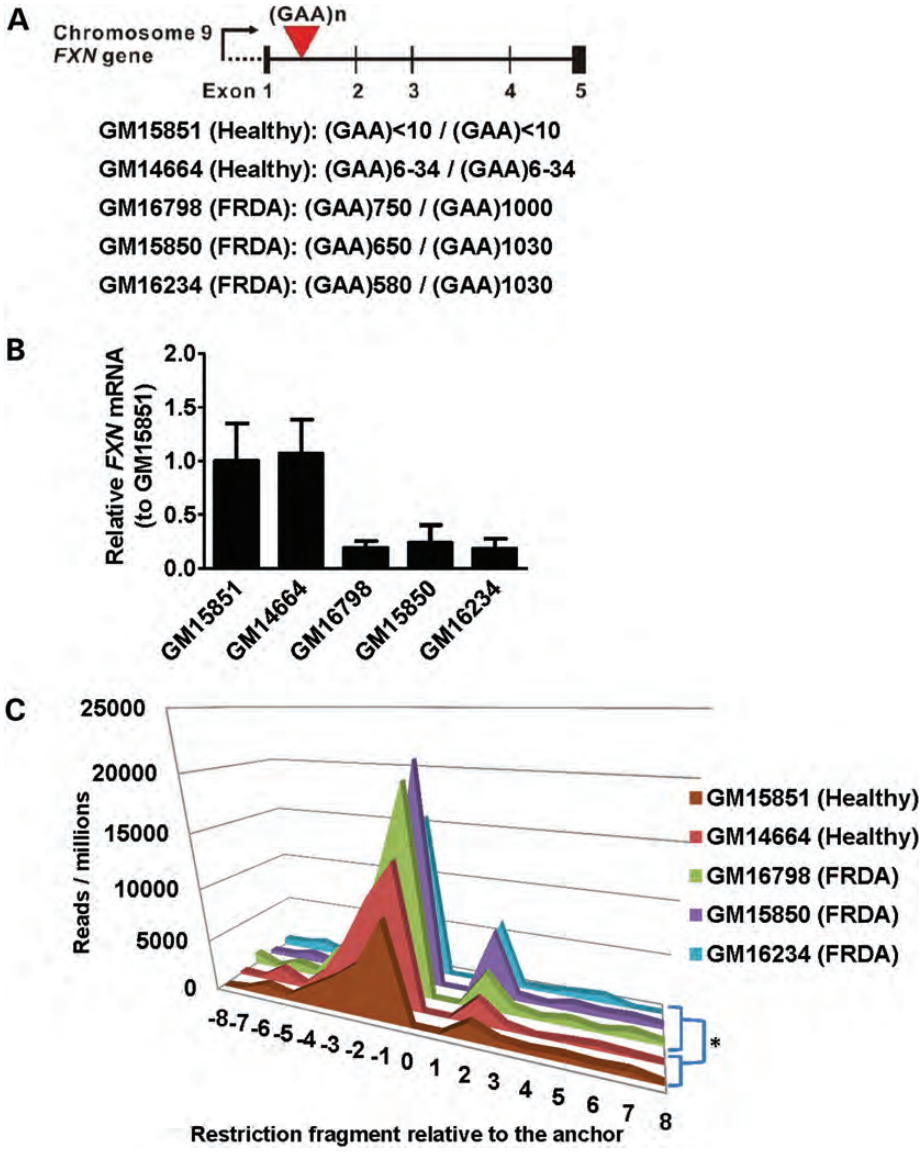

Figure 1. Increased interaction frequency within the *FXN* gene locus in FRDA cell lines. (**A**) Schematic diagram of the *FXN* gene locus with five exons (black boxes). The GAA repeats are located within intron 1 as indicated by the red inverted triangle. Chromosome conformation capture followed by a high-throughput sequencing (3C-seq) technique was used to determine the spatial organization of the *FXN* gene locus. (**B**) Frataxin mRNA expression levels were lower (~75%) in FRDA than in healthy control cells. (**C**) The GAA-repeat containing fragment was used as the anchor (denoted by 0) and the interaction frequency (with this anchor) was expressed as reads per millions. The *x*-axis represents the number of restriction fragments away from the anchor region (5′ upstream of the anchor indicated by a negative value and 3′ downstream represented by a positive value), i.e. fragment −8 located about 39 kb upstream and fragment +8 located about 45 kb downstream of *FXN* exon 1, respectively. Relatively stronger interactions were observed from patient-derived cells (GM16798, GM15850 and GM16234) when compared with healthy control (GM14664 and GM15851). The average interaction frequencies were ~1.5-fold higher in FRDA than healthy cell lines (*$P < 0.05$, Wilcoxon-matched pairs test).

RESULTS

A higher-order heterochromatic structure is formed at the *FXN* gene locus in FRDA

In recent years, accumulating data from different groups have demonstrated that alteration of post-translational histone modifications is an important underlying mechanism for *FXN* silencing in FRDA (4,10,12–14,18,34). The relationship between the chromatin architecture and histone modification marks in the *FXN* gene locus is likely to be important for understanding the silencing mechanism. We therefore investigated the spatial organization of the *FXN* gene locus using the 3C-sequencing method (28). EBV-transformed human lymphoblastoid cell lines derived from healthy or FRDA-affected individuals as denoted in Figure 1 were studied (Fig. 1A). The FRDA cell lines with large GAA-repeat expansions (e.g. >580 copies) showed strong *FXN* repression: mRNA expression in FRDA cell lines was <25% of the expression in the healthy controls (Fig. 1B). We then investigated whether this transcriptional repression alters the chromosome landscape of the *FXN* locus. Using an *Eco*RI restriction fragment containing exon 1 and the GAA region as

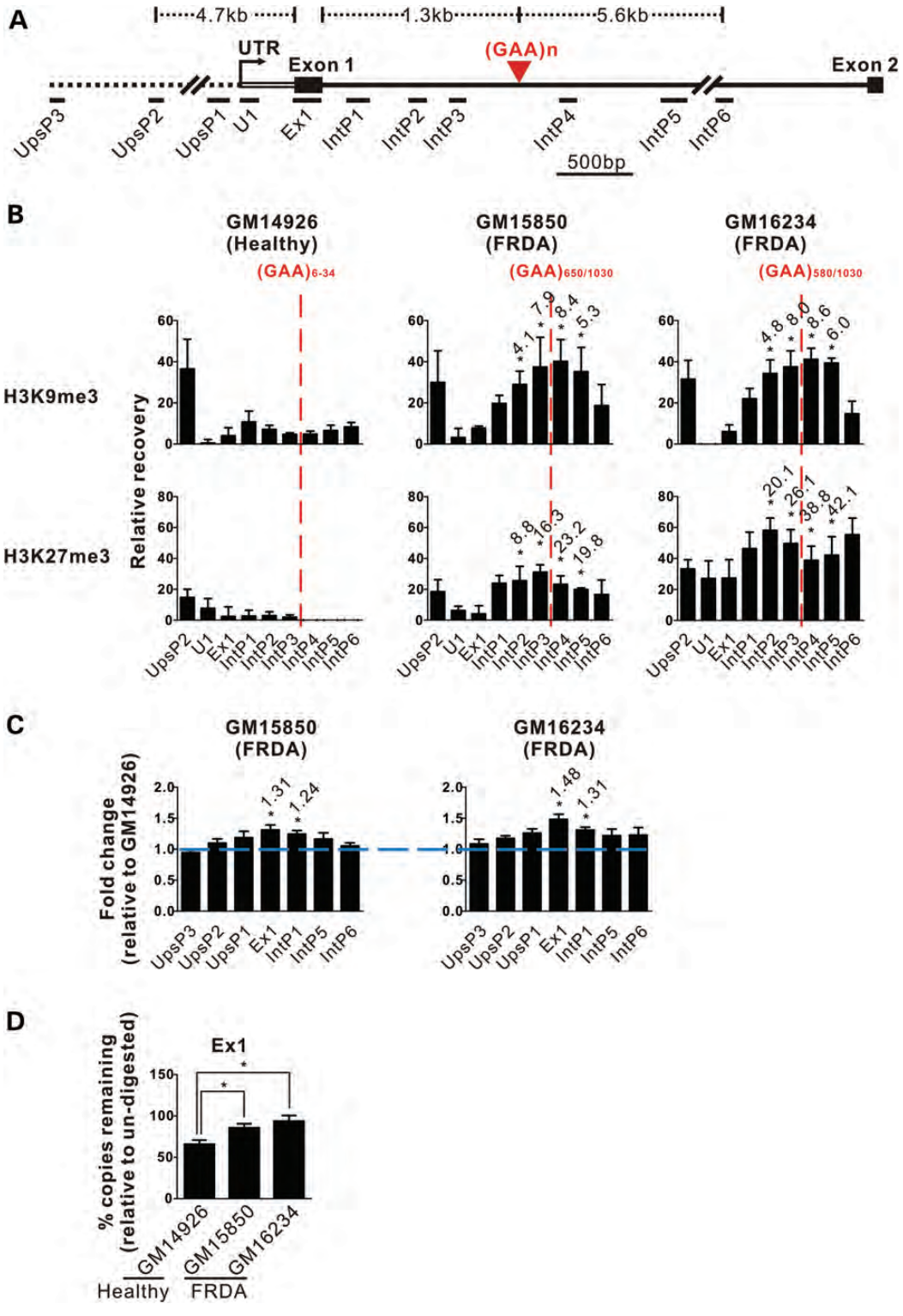

Figure 2. Histone H3 lysine 9 and 27 trimethylations are associated with a 'closed' chromatin structure in FRDA. (**A**) Schematic representation of the *FXN* gene locus investigated by ChIP and DNase I accessibility assays. The position and name of the primer sets used for both of these assays are indicated. (**B**) DNA pulled-down by ChIP with antibodies specific for either H3K9me3 or H3K27me3 were subjected to a qPCR. The signals were normalized to the histone H3 signal and expressed as relative recovery. Increased fold changes of the signal from FRDA compared with the same region in the healthy are shown on top of the data bars. ChIP was performed on three independent chromatin preparations. The data are presented as mean ± SEM. $^{*}P < 0.05$ (Student's *t*-test) comparing the same region as indicated (by asterisk) between FRDA and healthy control. The vertical broken line shows the location of the GAA repeats. (**C**) In FRDA, the *FXN* locus is less accessible to DNase I. Percentage of copies remaining after DNase I treatment for each of the regions investigated was assessed by a qPCR and the data are presented as the fold changes of the DNase I accessibility in FRDA compared with the healthy control (horizontal blue line). Data

the 'anchor' fragment (with fixed primers for generating the sequencing library), we detected interactions of this anchor with sites across the *FXN* genomic region ranging from −39 kb to +45 kb (relative to ATG of *FXN* exon 1) as denoted by an *Eco*RI restriction fragment −8 to +8 in Figure 1C. In general, the levels of relative cross-linking frequency were higher in FRDA cell lines as indicated by the higher peaks obtained compared with the healthy control (Fig. 1C). The mean values of interaction frequency were ∼1.5-fold higher in FRDA than healthy cell lines (Fig. 1C, $^{*}P < 0.05$, Wilcoxon-matched pairs test). This raises the possibility that a topological effect at the genomic level might be triggered by GAA-repeat expansion resulting in the stimulation of a more compact structure.

Heterochromatic marks at the histone H3 tail are associated with a 'closed' chromatin structure of the *FXN* locus in FRDA

Published data from our group have shown that GAA trinucleotide repeats can induce spreading of heterochromatin into proximal regions, and hence confer variegation of gene expression of a linked transgene *in vivo* (10). In line with our finding, trimethylation of lysine 9 in histone H3 (H3K9me3), a hallmark of heterochromatin, together with hypoacetylation of histones H3 and H4, has been found at the expanded GAA-repeat region and its immediate flanking regions in FRDA (4,12–14,18,35). To investigate whether the spreading of H3K9me3 along the *FXN* gene is correlated with gene silencing and a closed chromatin formation, we performed ChIPs with antibodies against H3K9me3 or H3K27me3 followed by a qPCR of the regions spanning from −5 kb to +7 kb of *FXN* exon 1 (Fig. 2A) in our cell line models. A statistically significant increase in H3K9me3 (ranging from 4.1- to 8.6-fold increase in patients compared with control) and H3K27me3 (ranging from 8.8- to 42.1-fold increase in patients compared with control) signals was observed in the regions flanking the GAA repeats in FRDA cells, suggesting that the heterochromatic structure is enriched in patient-derived cells when compared with healthy (Fig. 2B: IntP2-5; $^{*}P < 0.05$, Student's *t*-test). This result is in agreement with higher H3K9 and H3K27 trimethylation found at the *FXN* locus in FRDA-derived fibroblast cell lines (36). As these modifications are both well-known gene repression marks (37), our results support the hypothesis that GAA-induced heterochromatinization occurs in FRDA, thereby repressing the gene. Interestingly, we found that the levels of the heterochromatic marks decreased gradually with the distance from the GAA repeats towards exon 1 (denoted as IntP3 to U1 in Fig. 2B) in the FRDA cell lines. This result is consistent with the notion that GAA-repeat expansion can induce heterochromatin spreading towards the proximal regions (10). To directly address whether the heterochromatic structure we found in FRDA (Fig. 2B) can prohibit access to the *FXN* locus, we employed DNase I accessibility studies (30). No significant difference between FRDA cell lines and the healthy control could be observed at a region 8 kb upstream of *FXN* exon 1 (Fig. 2C: UpsP3). However, the fold increase of percentage of copies remaining in FRDA versus healthy control, following a 10 min incubation with DNase I, became obvious closer to the GAA repeats (Fig. 2C: UpsP2 to IntP1) and reached a maximum in exon 1 which is a region with DNase I hypersensitivity (HS) (Fig. 2C and D: Ex1 GM15850 = 1.31-fold and GM16234 = 1.48-fold increase in copies remaining compared with healthy control; $^{*}P < 0.05$, Student's *t*-test). HS sites reflect regions which are highly accessible in the nucleus. The presence of such an HS site agrees with DNase I HS mapping done as part of ENCODE on various cell models including EBV-transformed lymphoblastoid cells (38). Figure 2D shows the data obtained from Ex1 and reveals the increase in DNA copies remaining in FRDA compared with healthy cells after DNase I treatment ($^{*}P < 0.05$, Student's *t*-test). A similar DNase I accessibility pattern was also obtained after 20 min exposure to DNase I (Supplementary Material, Fig. S1). These results show directly that GAA-repeat-induced heterochromatin appears to prohibit access to the *FXN* locus in FRDA. It follows that antagonizing heterochromatin formation might lead to increased accessibility and derepression of the *FXN* gene.

Nicotinamide, an HDAC class III inhibitor, upregulates *FXN* gene expression

Several therapeutic strategies involving iron chelators and antioxidants have been developed for FRDA, but unfortunately they have had only limited effect in alleviating the neurological consequences or the cardiomyopathy, which is a major cause of death in FRDA patients (5). Recently, various types of HDACi's have been shown to relieve repression of the *FXN* gene in different FRDA models (12,16–19). In this report, we investigated whether the readily available HDACi nicotinamide could restore *FXN* mRNA expression in FRDA. We first tested the effect of nicotinamide on the EBV-transformed lymphoblastoid cell lines. Modest 1.5- to 1.8-fold up-regulation of *FXN* mRNA levels was obtained in patient-derived cell lines (Supplementary Material, Fig. S2) with relatively little effect on *FXN* expression in the normal control cell line. To assess the effect of nicotinamide under more physiological conditions, fresh primary lymphocytes derived from FRDA-affected or normal healthy individuals were treated. A small effect (∼2-fold increase) in *FXN*

collected after 10 min digestion are shown and a similar DNase I accessibility pattern was obtained from another time point (20 min) (Supplementary Material, Fig. S1). The amount of template DNA was normalized to a DNase I insensitive region within the NfM and the data were expressed relative to the signals from the healthy control. The DNase I sensitivity assay was performed on three independent nuclei preparations. The data are presented as mean ± SEM. $^{*}P < 0.05$ (Student's *t*-test) comparing the same region as indicated (by asterisk) between FRDA and healthy control. (**D**) The percentage copies remaining are higher in patients when compared with healthy indicating reduced accessibility. DNase I sensitivity results at Ex1 are presented as percentage of copies remaining after 10 min digestion from each cell line compared with its undigested control. The assay was performed on three independent nuclei preparations and data are presented as mean ± SEM. $^{*}P < 0.05$ (Student's *t*-test).

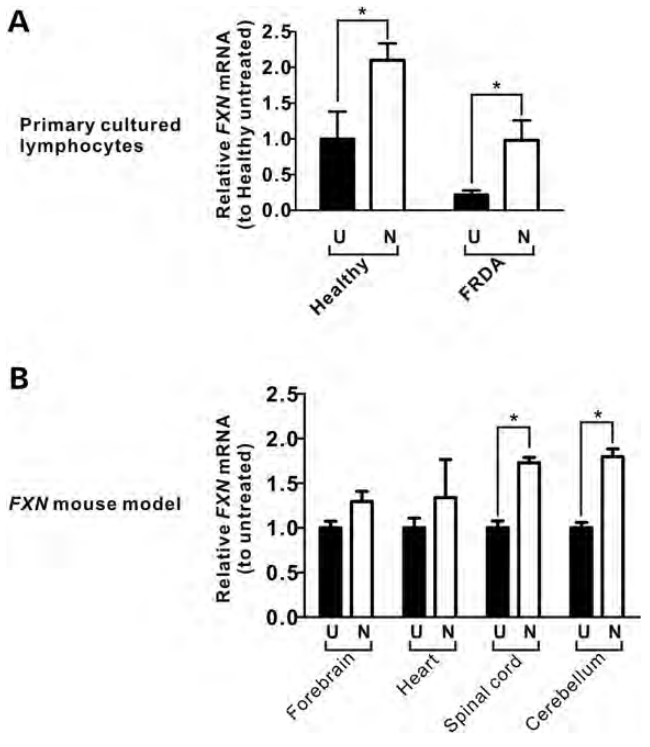

Figure 3. Nicotinamide can reactivate the silenced *FXN* gene in different FRDA models. *FXN* mRNA expression levels before (U, untreated) and after nicotinamide treatment (N) was determined by a qRT–PCR. The mRNA expression levels were normalized to β-actin. (**A**) Blood donated from FRDA patients and healthy individuals was used for lymphocyte isolation and treated with nicotinamide for 3 days before *FXN* mRNA measurement. The data are presented as mean ± SEM. Five healthy and six FRDA patients were recruited. $^{*}P < 0.05$ (Student's *t*-test). The qPCR was performed in duplicate. (**B**) FRDA transgenic mice were treated with nicotinamide by a daily intraperitoneal injection for 6 days before tissue collection. Values are shown relative to the vehicle-treated transgenic mouse for each of the tissues. The data are presented as mean ± SEM, $n = 3$. The qPCR was performed in duplicate. $^{*}P < 0.05$ (Student's *t*-test).

mRNA level was produced for healthy primary cells after nicotinamide treatment suggesting that minor chromatin effects might occur at the healthy *FXN* locus. Notably, the increase in *FXN* mRNA level in FRDA individuals was much larger (~4.5-fold) (Fig. 3A; $^{*}P < 0.05$, Student's *t*-test).

Since FRDA mainly affects the nervous systems and heart and these tissues are difficult to obtain from patients, we treated human FRDA transgenic mice (39) with nicotinamide for 6 days. Clinically relevant tissues including those from the heart, spinal cord and cerebellum were collected in order to measure *FXN* mRNA expression levels. Obvious increases of *FXN* mRNA expression were found in all FRDA-relevant tissues and the most substantial increases, in terms of fold up-regulation, were observed in spinal cord and cerebellum with ~1.8-fold up-regulation of *FXN* after nicotinamide treatment (Fig. 3B; $^{*}P < 0.05$, Student's *t*-test). Taken together, these results strongly suggest that nicotinamide can reactivate the silenced *FXN* gene in both human FRDA cells and *in vivo* transgenic FRDA models. Thus, nicotinamide acts preferentially on FRDA-affected subjects consistent with a possible de-condensation of the more heterochromatic structure induced by the GAA-repeat expansion in FRDA compared with the healthy control.

Nicotinamide decreases H3K9 and H3K27 trimethylations at the *FXN* gene in FRDA

To investigate further the mechanism whereby nicotinamide induces *FXN* expression, we measured the epigenetic changes by ChIP with antibodies against H3K9me3 and H3K27me3. Since human primary cultured lymphocytes are a better physiological model than lymphoblastoid cell lines, ChIP experiments were performed on primary lymphocytes derived from FRDA patients and healthy individuals. H3K9me3 levels were higher (>3-fold) throughout the investigated regions, from Ex1 to IntP5, in FRDA patients than in healthy controls (Fig. 4A: upper panel, untreated healthy versus untreated FRDA; $^{\wedge}P < 0.05$, Wilcoxon-matched pairs test), confirming that heterochromatinization is associated with GAA-repeat expansion in FRDA fresh primary cells (10). Treatment with nicotinamide produced little effect in the healthy control, although nonsignificant reductions of H3K9me3 signals were observed at Ex1, IntP1, IntP3, IntP4 and IntP6 (Fig. 4A, upper panel, healthy). Strikingly, treating the primary cells from patients with nicotinamide led to a substantial decrease (>2.9-fold) in H3K9me3 levels throughout the regions investigated, with the largest decrease occurring at exon 1 (Fig. 4A: upper panel, FRDA; $^{\#}P < 0.05$, Wilcoxon-matched pairs test). Interestingly, the level of H3K9me3 was higher in exon 1 in primary lymphocytes compared with the other cell types tested; this implies cell-type specific differences in heterochromatinization. Similar to the result from H3K9me3 ChIP, the healthy primary cells showed no statistically significant difference in H3K27me3 levels as a result of nicotinamide treatment (Fig. 4A, lower panel, healthy). However, there was a clear-cut reduction (>1.56-fold decrease) in H3K27me3 in nicotinamide-treated FRDA cells compared with untreated control (Fig. 4A, lower panel, FRDA; $^{\#}P < 0.05$, Wilcoxon matched pairs test). To investigate whether nicotinamide has the same effect in one of the tissues affected by FRDA, cerebellum from human FRDA transgenic mice was analyzed for H3K9me3 and H3K27me3 using ChIP. Consistent with the results obtained from human primary cells, both H3K9 and H3K27 trimethylation levels were substantially reduced by >2.1-fold and >1.6-fold, respectively, within the *FXN* gene (Ex1 to IntP5 regions) after nicotinamide treatment (Fig. 4B, $^{\#}P < 0.05$, Wilcoxon-matched pairs test).

Nicotinamide increases histone acetylation at the *FXN* gene in FRDA

Because the chromatin landscape is influenced by the interplay between methylation and acetylation of histone molecules, histone acetylation marks were also determined. We performed ChIP with antibodies specific for acetylated histones H3 and H4, respectively. As primary cultured lymphocytes from FRDA patients showed the highest sensitivity to nicotinamide treatment, we focused on determining the possible changes of the histone acetylation profile in patients. Overall histone H3 and H4 acetylations were shown to be up-regulated

(H3ac >1.99-fold and H4ac >1.81-fold increase) along the investigated regions after a 3-day treatment with nicotinamide (Fig. 4C; $^{\#}P < 0.05$, Wilcoxon matched pairs test). These results suggested that nicotinamide could decondense the 'closed' chromatin structure induced by the GAA-repeat expansion in FRDA and thereby, at least partly, reactivate the silenced *FXN* gene.

Nicotinamide increases DNase I accessibility at the *FXN* gene in FRDA

In order to directly evaluate the effectiveness of nicotinamide in rendering the pathologically silenced *FXN* gene accessible to protein factors, we determined the changes in DNase I accessibility upon nicotinamide treatment either in healthy or in FRDA primary cells. The results showed that DNase I accessibility in both Ex1 and IntP1 regions were increased by 20 and 40%, respectively, in FRDA (Fig. 4D). It is worth noting that the increase in DNase I accessibility was much greater in patients compared with control: at Ex1 it was >3.5-fold and at IntP1 >2.1-fold ($^{*}P < 0.05$ in both cases, Student's *t*-test). In contrast, the control upstream UpsP2 region showed no significant difference between FRDA and healthy cells (Fig. 4D: UpsP2) after nicotinamide treatment. This result provides direct evidence that nicotinamide acts selectively in FRDA to increase accessibility in regions adjacent to the expanded GAA-repeat sequence.

Nicotinamide decreases interaction frequency at the *FXN* gene in FRDA

As increased association of genomic elements at the *FXN* gene locus was detected by our 3C-sequencing experiment in FRDA (Fig. 1), it was of interest to determine whether nicotinamide could decrease the interaction frequency as this would suggest decompaction. Fragment number 2 from the 3C-seq was employed for studying the effect of nicotinamide treatment as it showed the biggest difference in interaction frequency between FRDA and healthy cells (Fig. 1C). Primary lymphocytes from patients were isolated and treated with nicotinamide in the same way as for the ChIP experiment. The cells were then harvested and processed according to the 3C protocol (see Materials and Methods). A 3-fold reduction in the relative cross-linking frequencies was observed in nicotinamide treated cells when compared with the untreated control (Fig. 4E, $^{*}P < 0.05$, Student's *t*-test). Taken together with the up-regulatory effect of nicotinamide on the *FXN* gene (Fig. 3), the reductions in heterochromatic marks and the local genomic interaction frequency suggest that nicotinamide helps to 'disperse' the heterochromatic structure in fresh lymphocytes derived from FRDA patients.

Nicotinamide treatment can normalize the biomarkers associated with FRDA in primary cells

To investigate the efficacy of nicotinamide treatment using our *ex-vivo* primary cell model, we performed high-throughput RNA sequencing on libraries generated from untreated and nicotinamide-treated samples. Significantly differentially expressed (DE) genes were identified by DEseq analysis and only a small proportion of genes, 4.3% of all the genes identified in the analysis, were significantly changed (FDR < 0.05) after nicotinamide treatment. Reactome pathway analysis using the GOseq package was employed to identify the biological pathways affected by the DE genes upon nicotinamide treatment (40). Importantly, from the toxicity point of view, there was a lack of changes related to apoptotic and tumorigenesis pathways, suggesting that nicotinamide-induced apoptosis and adverse oncogenic effects are very unlikely. From the Gene Ontology (GO) analysis, a number of GO terms were related to the immune system (e.g. immune response, innate immune response and regulation of the immune system process) which is consistent with the Reactome pathway analysis. This was not surprising as nicotinamide has been shown to play a role in MHC expression in mammalian systems (41) and previous studies in mice and humans have been done where large doses of nicotinamide were given long term in an attempt to prevent autoimmune diabetes in at-risk individuals (33,42–44). Full lists of the Reactome pathway analysis are shown in Supplementary Material, Table S2.

Chronic deficiency of frataxin protein in FRDA patients triggers alterations in gene expression. Previously, a set of biomarkers (P77) associated with frataxin deficiency in FRDA have been shown to be sensitive to the treatment with a pimelic *o*-aminobenzamide compound (32). We employed this P77 set of biomarkers as a proxy to reflect a potential correction of these dysregulated genes upon nicotinamide treatment (32). This was done by comparing the fold change in gene expression obtained in primary lymphocytes before and after nicotinamide treatment with the difference between the asymptomatic carrier and FRDA patients previously described (32) (Supplementary Material, Fig. S3). A total of 70 genes out of 77 from the biomarker list were found to be sensitive to the treatment and ~67% of the biomarkers were normalized by nicotinamide treatment towards healthy levels as highlighted in gray color in Supplementary Material, Figure S3. Notably, 53 and 40% of the FRDA-related biomarkers are corrected by greater than 50% when compared with asymptomatic carriers and healthy controls, respectively (Fig. 5B, dark red colored bars). These results raise the possibility that nicotinamide treatment might be able to ameliorate gene expression abnormalities related to *FXN* deficiency in FRDA.

DISCUSSION

It has been clearly demonstrated with chromatin immunoprecipitation approaches that repressive heterochromatin is formed in the flanking regions of the GAA-repeat expansion in FRDA (4,12–14). We report here the results from 3C-seq and DNase I accessibility assays that higher-order chromatin organization is found together with heterochromatic histone marks in FRDA. Recent studies using 3C-based techniques have mainly focused on transcriptional activation rather than heterochromatin-mediated silencing (45). Interestingly, here, we found that the cross-linking frequency along the *FXN* gene locus is higher in FRDA-derived cells compared with the healthy control, suggesting that GAA-associated heterochromatinization correlates with an overall increase in

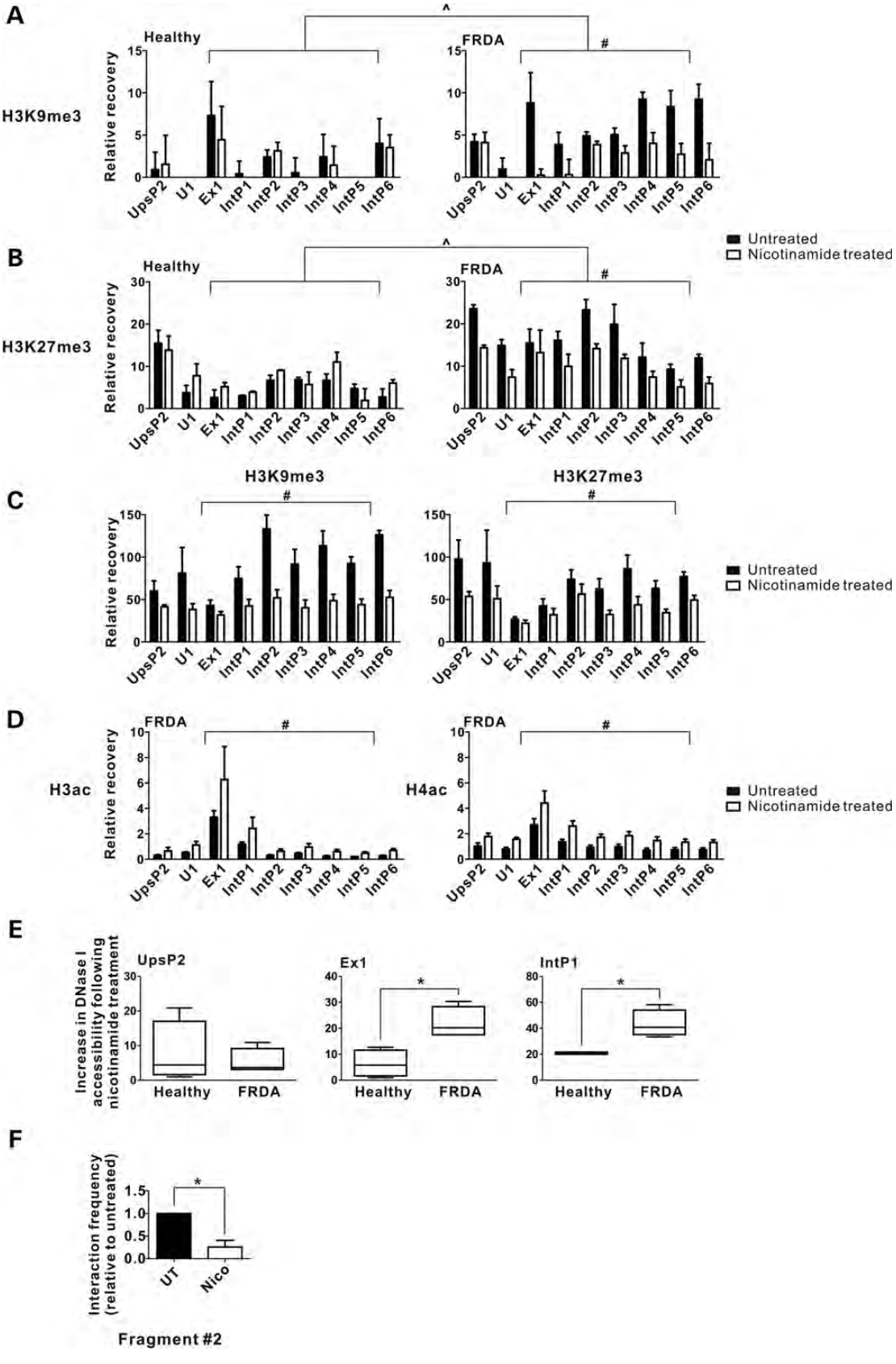

Figure 4. Nicotinamide reduces heterochromatic marks and decondenses chromatin at the *FXN* gene in FRDA. (**A**) Primary cultured lymphocytes derived from FRDA patients and healthy individuals were treated with nicotinamide and compared with their untreated control. H3K9me3 and H3K27me3 ChIPs were

interactions within the vicinity of the *FXN* locus. It is tempting to speculate that the GAA-triplet repeats in the anchor fragment nucleate heterochromatin formation bringing the neighburing nucleosomes closer to each other (11), thereby promoting interaction between distal DNA elements (Fig. 6). Such dense nucleosomal packaging is a feature of heterochromatin (46,47) and thought to be stimulated by H3K9me3-modified nucleosomes being linked by HP1 dimers (48,49) and is, therefore, implicated in the formation of a higher-order heterochromatic structure (50). Thus, the increase of this interaction frequency triggered by GAA-repeat expansion could simply be the consequence of the formation of a heterochromatic structure in FRDA.

To determine whether the GAA-repeat-induced heterochromatin is refractory to the transcriptional machinery, we employed a modified DNase I accessibility assay to further investigate the chromatin landscape in the anchor region. Our data demonstrated that DNase I accessibility is decreased in FRDA versus the healthy control (Fig. 2C, Ex1 and IntP1), indicating that condensed heterochromatin, presumably contributed by H3K9 and K27 trimethylations, can prohibit access of DNase I to the *FXN* locus.

Taken together, our results suggest a mechanism, whereby heterochromatin both compartmentalizes the affected locus and prohibits access to it. Such effects are likely to be crucial for setting up a silent locus and dependent on many factors, including the formation of triplex-DNA and DNA–RNA hybrid structures (7,9), hindrance to the transcription factor (e.g. CTCF) binding at the *FXN* promoter (36), and DNA hypermethylation in the region 5′ upstream of the repeat (13,14).

Previous studies using HDACi to treat FRDA models (12,16–19) provided data which support the hypothesis that an HDACi could shift the equilibrium of the chromatin status towards a transcriptionally active *FXN* locus (11). In the present study, we used nicotinamide, because it is an off-the-shelf medication that has been used at high dosage for a variety of therapeutic applications over the past 40 years (33). Our results show that nicotinamide can up-regulate *FXN* expression in different FRDA models comprising EBV lymphoblastoid cell lines, *ex-vivo* human primary cultured lymphocytes and a transgenic mouse model of FRDA. The greatest up-regulation was seen in *ex-vivo* primary cells which provide a more physiologically relevant model than EBV lymphoblastoid cell lines. Importantly, the *FXN* gene was more sensitive to up-regulation by nicotinamide in FRDA cells than in healthy cells. This difference is likely to be due to the increased GAA-repeat length in FRDA leading to pathological heterochromatinization which can be antagonized by HDAC inhibition. By treating human FRDA transgenic mice with nicotinamide, we found that treatment for 6 days was effective in clinically relevant tissues (heart, spinal cord and cerebellum) *in vivo*. In conclusion, our results show that nicotinamide preferentially acts on FRDA alleles to increase *FXN* expression to the level of asymptomatic heterozygotes (~40% of normal levels) raising the possibility that it might be of benefit in preventing disease progression in affected tissues (51). However, the dose of nicotinamide used in the present study on our cell models was much higher than the recommended daily dose of this vitamin (~16 mg per day) in human. One must be cautious about the use of nicotinamide as more work needs to be done before it should be considered a potential therapy for FRDA.

Our *in vitro* and *in vivo* data obtained by ChIP with H3K9me3 and H3K27me3 antibodies (Fig. 4) demonstrated that treatment with nicotinamide antagonizes heterochromatinization as shown by significant reduction of the histone trimethylations occupancy at the *FXN* locus. To the best of our knowledge, this is the first demonstration that the accumulation of H3K9me3 coincides with H3K27me3 induced by GAA expansion in FRDA *ex-vivo* and *in vivo* models and is consistent with the data previously obtained from lymphoblastoid cell lines (Fig. 2B). We also showed that treating several different FRDA models with nicotinamide can effectively reduce the heterochromatinization induced by hyperexpanded GAA repeats and that this results in *FXN* mRNA up-regulation. Our results suggest that both H3K9 and K27 trimethylations are important for *FXN* silencing in FRDA. However, this result seems to differ from a previous report, claiming that H3K9 methylation is dispensable for *FXN* silencing (4). This discrepancy may be due to the fact that, in their report, inhibition of G9a (a histone H3K9 methytransferase) with BIX-01294 would only reduce the levels of H3K9me2/me3, potentially leaving other heterochromatic marks unchanged. The 'closed' chromatin landscape which is occupied by other histone modifications, for example H3K27me3 (shown here), might therefore remain to repress the *FXN* gene upon BIX-01294 treatment. Notably, the authors point out in their paper that BIX-01294 treatment actually increased *FXN* mRNA levels in an FRDA cell line

performed in the same manner as in the previous section (Fig. 2). Combined H3K9me3 and H3K27me3 signals from Ex1 to IntP5 are higher in untreated FRDA when compared with the untreated healthy cells, respectively. $^{\wedge}P < 0.05$, Wilcoxon-matched pairs test. Both H3K9me3 and H3K27me3 heterochromatic marks are reduced upon nicotinamide treatment. ChIP data are presented as mean ± SEM, $n = 3$ healthy; $n = 3$ FRDA. The qPCR was performed in duplicate. Statistical analysis was performed by comparing combined signals from Ex1 to IntP5 in FRDA treated with the untreated control. $^{\#}P < 0.05$, Wilcoxon-matched pairs test. (**B**) Nicotinamide was given to FRDA transgenic mice for 6 days before cerebellum was taken for ChIP experiment. The results are presented as mean ± SEM, $n = 3$. Statistical analysis was performed by comparing combined signals from Ex1 to IntP5 in nicotinamide treated samples with the untreated control. $^{\#}P < 0.05$, Wilcoxon-matched pairs test. (**C**) Mapping of the possible changes of histone acetylation upon nicotinamide treatment in FRDA, ChIP was performed with antibodies against histones H3 and H4 acetylation marks. The values are presented as mean ± SEM, $n = 2$ healthy; $n = 2$ FRDA. The qPCR was performed in duplicate. Statistical analysis was performed by comparing combined signals from Ex1 to IntP5 in nicotinamide treated with the untreated control. $^{\#}P < 0.05$, Wilcoxon-matched pairs test. (**D**) Relative increase of DNase I accessibility by nicotinamide treatment in primary cultured lymphocytes. The increase of DNase I accessibility produced by nicotinamide treatment was calculated by subtracting the signal following nicotinamide treatment from the signal obtained without treatment. $n = 2$ healthy; $n = 2$ FRDA. The qPCR was performed in triplicate. $^{*}P < 0.05$ (Student's *t*-test). (**E**) 3C-qPCR analysis of the interaction frequency after nicotinamide treatment on fragment number 2 (refer to the fragment labeling in Fig. 1) in patient derived primary lymphocytes. The result is presented as mean ± SEM, $n = 2$. The qPCR was performed in triplicate. $^{*}P < 0.05$ (Student's *t*-test).

A

Reactome ID:	Description	FDR
168256	Immune System	2.88E-34
1280215	Cytokine Signaling in Immune system	4.71E-23
913531	Interferon Signaling	1.95E-20
877300	Interferon gamma signaling	3.23E-16
909733	Interferon alpha/beta signaling	3.32E-15

Gene Ontology ID:	Term	Ontology	FDR
GO:0006955	Immune response	Biological process	1.59E-81
GO:0006952	Defense response	Biological process	6.61E-81
GO:0002376	Immune system process	Biological process	4.01E-80
GO:0050896	Response to stimulus	Biological process	6.57E-71
GO:0006950	Response to stress	Biological process	1.36E-64
GO:0045087	Innate immune response	Biological process	4.20E-55
GO:0002682	Regulation of immune system process	Biological process	2.72E-47
GO:0042221	Response to chemical stimulus	Biological process	3.83E-47
GO:0009611	Response to wounding	Biological process	2.28E-44
GO:0051716	Cellular response to stimulus	Biological process	4.01E-44

B

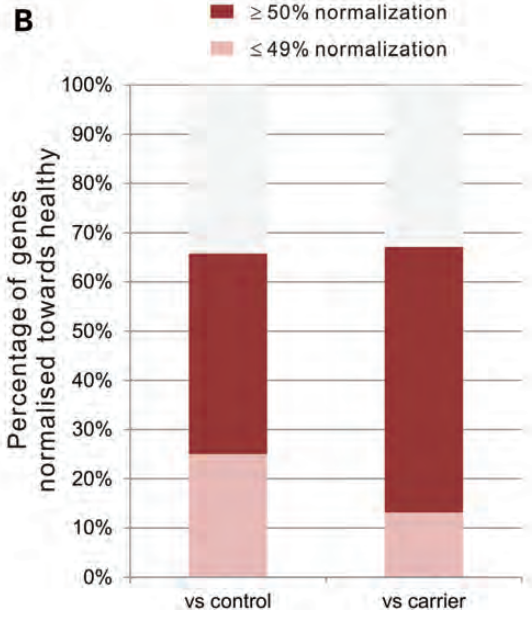

Figure 5. Nicotinamide did not result in large-scale changes in gene expression but corrected FRDA biomarkers. (**A**) Reactome pathway analysis of the significantly altered genes was performed to identify molecular pathways associated with nicotinamide. Significantly enriched pathways are shown in the upper panel. GO analysis was performed as mentioned in Materials and Methods. The 10 most significantly enriched GO terms are shown in the lower panel. (**B**) Seventy genes from the P77 biomarker set previously identified (32) were found to be sensitive to the drug treatment (Supplementary Material, Fig. S3). Stack bar plot showing the percentage of genes with different degrees of correction of the biomarkers due to the deficiency of frataxin protein in FRDA when compared with either the carrier or the control. See Materials and Methods for the calculation of the trend normalization. The affected genes were divided into two categories showing the percentage of genes normalizing to at least 50% ($\geq$50% normalization) and $<$49% ($\leq$49% normalization) of asymptomatic controls, respectively. Analysis was done on primary lymphocytes derived from patients after nicotinamide treatment ($n = 2$).

showing a ~1.5-fold *FXN* up-regulation (4). This is similar to the result shown here after nicotinamide treatment of lymphoblastoid cell lines, where we show 1.5- to 1.8-fold up-regulation (Supplementary Material, Fig. S2); our results reveal that lymphoblastoid cell lines are much less sensitive to HDAC inhibition than *ex vivo* or *in vivo* responses (Fig. 3). Nevertheless, even 1.5-fold up-regulation could be of therapeutic benefit, while excessive expression might be toxic. Nicotinamide seems likely to have some advantages over the other HDACi treatments as we have shown here that it could reduce H3K9me3 and H3K27me3 concomitantly and result in *FXN* reactivation via apparent 'de-condensation' of the heterochromatic structure. One of the possible mechanisms of action of nicotinamide is by inhibiting SIRT1 (24), which has been shown to promote heterochromatin formation by histone deacetylation, H1b recruitment and promoting the loss of transcriptionally active marks (e.g. H3K79me2) (26). More recently, Reinberg *et al.* demonstrated that SIRT1 is also responsible for activating SUV39H1 by deacetylating it, resulting in H3K9 trimethylation deposition (27). Thus, inhibition of SIRT1 would be expected to result in H3K9 demethylation and histone acetylation both of which we found in this study upon nicotinamide treatment.

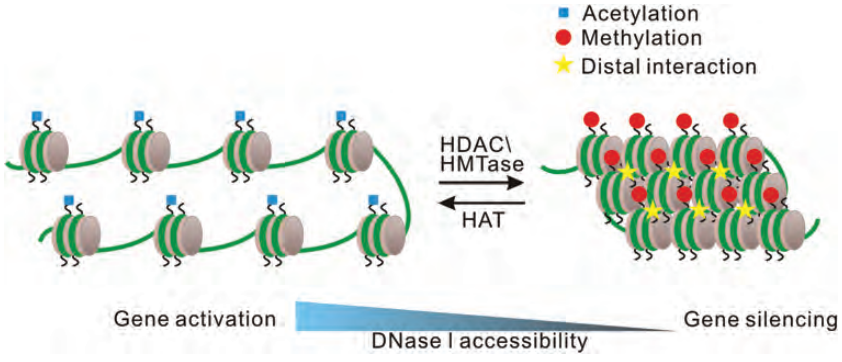

Figure 6. Higher-order chromatin structure induces distal DNA interaction and reduces DNase I accessibility in FRDA. The chromatin organization of an active *FXN* gene is shown on the left with nucleosomes mainly composed of acetylated histone molecules. In FRDA, hyperexpanded GAA repeats nucleate heterochromatin formation and thereby push the pathway towards the right side with nucleosomes dominated by various types of methylations. In the higher-order heterochromatic structure, nucleosomes are compartmentalized into a condensed space. This might promote genomic regions, which are normally located far away from each other in the gene activation stage, bridging with their partner (yellow star: distal interaction). Once the condensed structure is stabilized by heterochromatin protein 1, accessibility of transcriptional machinery will be prohibited as indicated by the decrease of DNase I accessibility at the bottom of the model.

In this report, we show that nicotinamide can reduce pathological heterochromatin at the *FXN* gene and reactivate it in a mouse model *in vivo* and in primary cells from patients. This reveals a potential novel treatment for FRDA, a currently incurable and frequently devastating disease, but of course much work remains to be done on the safety and tolerability of this drug in patients before pursuing clinical studies for efficacy.

MATERIALS AND METHODS

Cell culture

EBV-transformed lymphoblastoid cells GM14926, GM14664, GM15850, GM15851, GM16234, GM16798 were purchased from the National Institute of General Medical Sciences Human Genetic Cell Repository at the Coriell Institute, Camden, NJ, USA. Lymphoblastoid cell lines were grown in RPMI 1640 (PAA) medium with 2 mM L-glutamine and 10% fetal calf serum (PAA) and supplemented with 1× penicillin/streptomycin solution (GIBCO) at 37°C in 5% CO_2. Primary lymphocytes from healthy individuals and FRDA patients were isolated from the blood samples using a Ficoll-Hypaque TM gradient (Sigma) following the manufacturer's protocol. Human blood samples were obtained from FRDA patients and healthy individuals in accordance with UK Human Tissue Authority ethical guidelines. Primary lymphocytes were cultured under the same conditions as for the EBV-transformed lymphoblastoid cell lines.

Transgenic mouse model

Mouse forebrain, cerebellum, heart and spinal cord were collected from previously described *FXN* YAC (YG8) transgenic mouse model (52).

Chromosome conformation capture (3C)

The 3C protocol was adapted from Hagege *et al*. (28) with some modifications. 1×10^7 cells were cross-linked with 1% formaldehyde in 10 ml culture medium for 10 min at room temperature. The reaction was quenched by the addition of glycine to 0.125 M. Nuclei were harvested by lysis of the cells in 1 ml ice-cold lysis buffer [150 mM NaCl, 50 mM Tris–HCl (pH 7.5), 5 mM EDTA, NP-40 (0.5% v/v), Triton-X-100 (1.0% v/v)] with a 1× protease inhibitor cocktail solution (Sigma) plus 0.5 mM PMSF. Nuclei were resuspended in 0.5 ml *Eco*RI restriction buffer (NEB) with 0.3% SDS and incubated for 1 h at 37°C with agitation. Triton X-100 was added to 2% (v/v) and incubated for 1 h at 37°C with agitation. Cross-linked nuclei were digested overnight at 37°C with 400 U *Eco*RI. Addition of SDS to 1.6% to stop restriction and further incubated at 65°C for 20 min with agitation. The reaction was diluted with 7 ml ligation buffer with Triton-X-100 and incubated for 1 h at 37°C prior addition of 100 U of T4 DNA ligase (Fermentas) for 4 h at 16°C and then 30 min at RT. Reverse cross-linking was done by adding 600 mg Proteinase K and incubated at 65°C overnight. After RNase A digestion, DNA was purified by phenol/chloroform extraction. The DNA pellet was resuspended in 150 µl 10 mM Tris-Cl (pH 7.5). Real-time PCR was performed in triplicate using custom dual-labeled fluorogenic probe (Sigma). The relative cross-linking frequency of the targeting restriction fragment was calculated by normalizing to *FXN* random template control (prepared according to 3C technique (53) with BAC clone carrying *FXN* gene locus) and endogenous control, ACTA2. Sequences of the 3C qPCR primers are listed in Supplementary Material, Table S1.

3C high-throughput sequencing experiment

3C-seq templates were generated as for 3C using *Eco*RI. After ligation and purification, the restriction fragments ligated to the anchor region (containing *FXN* exon 1) were amplified by an inverse PCR as described (54). Therefore, the anchor region was defined as fragment number 0 in the figure. One microgram of template was amplified per reaction by using a Phusion High-Fidelity PCR kit (Finnzymes; Cat.# F-553S) and primers incorporated with different indexes. Primer

sequences were listed in Supplementary Material, Table S1. The libraries were processed according to manufacturer's instructions (Illumina Inc.). An R package (r3Cseq) was employed for determining interaction frequency and expressed as reads per million (RPM) per each restriction fragment (55). Signal from fragment number 1 (the first fragment downstream of exon 1) was removed as the background noise signal was too high.

DNase I accessibility assay

5×10^7 cells were harvested and washed with 5 ml ice cold PBS and resuspended in 5 ml cold RSB buffer (10 mM Tris–HCl, pH 7.5, 10 mM NaCl, 3 mM $MgCl_2$). Ice cold RSB-NP40 buffer (RSB with 0.5% (v/v) Nonidet *P*-40) was added to lyse the cell membrane and the reaction was stopped by addition of 2.2 volume of RSB buffer. Nuclei pellet was resuspended in fresh RSB at 1×10^8 nuclei/ml density. DNase I at concentration of 0.01 U/μl was used for a 250 μl digestion reaction. 50 μl of digestion sample was collected per 1, 5, 10 and 20 min (as the time points) intervals and mixed with 50 μl 2× DNase I stop buffer [2 mM Tris–HCl, pH 8.0, 600 mM NaCl, 10 mM EDTA, 1% (w/v) SDS]. 150 μl of lysis buffer [100 mM Tris–HCl, pH 8.5, 5 mM EDTA, 200 mM NaCl, 0.2% (w/v) SDS, 1.5 mg/ml protease K] was then added and incubated at 55°C overnight. DNA was purified by phenol/chloroform extraction. Quantification of percentage copy remaining by qPCR was performed as described previously (30) with normalization to neurofilament gene (NfM) (56) as the endogenous control. A real-time qPCR was carried out in the same way as described in the following ChIP section. qPCR primer sequences are provided in the Supplementary Material, Table S1. In Figure 4C, the increase of DNase I accessibility produced by nicotinamide treatment was calculated by subtracting the signal following nicotinamide treatment from the signal obtained without treatment.

Nicotinamide treatment

10 mM nicotinamide (Fluka:Sigma) was used to treat 1.8×10^7 EBV-transformed lymphoblastoid cells in 36 ml culture medium for 16 h. Primary lymphocytes at a cell density of 1×10^7 cells/ml were treated with 10 mM nicotinamide for 3 days. Culture medium with or without (untreated as control) nicotinamide was changed every 24 h incubation. For nicotinamide treatment of the transgenic mice, 750 mg/kg of nicotinamide (dissolved in physiological saline) was given to mice by intraperitoneal injection once per day for 6 days. Untreated control was done by injecting the mice with physiological saline.

RNA extraction and qRT-PCR

Total RNA was isolated from 1×10^6 cultured cells using Trizol (Invitrogen) and reverse transcribed using the ThermoScript™ RT–PCR system (Invitrogen) by following the manufacturer's instructions. We performed a qRT–PCR using the SYBR® Green JumpStart™ Taq ReadyMix™ (Sigma). *FXN* mRNA levels are expressed relative to β-actin mRNA. All values are expressed as mean ± SEM. Statistical analysis was performed on three independent qRT–PCR experiments for each biological sample.

Chromatin immunoprecipitation (ChIP)

We performed chromatin immunoprecipitation as previously described with minor modification to our experimental models (31). Cells were cross-linked for 15 min with 1% formaldehyde at RT, quenched with glycine and followed by sonication (Bioruptor, Diagenode). The average DNA fragment length after sonication was between 200 and 400 bp. Immunoprecipitation was done by using commercially available antibodies: histone H3 (Abcam) Cat.#Ab1791, H3K9 trimethylation (Millipore) Cat.#17-625, H3K27 trimethylation (Abcam) Cat.#Ab6002, H3 acetylation (acetyl K9 + K14 + K18 + K23 + K27) (Abcam) Cat.#Ab47915 and H4 acetylation (acetyl K5 + K8 + K12 + K16) (Millipore) Cat.#06-866. The amount of *FXN* DNA immunoprecipitated was determined using an SYBR® Green JumpStart™ Taq ReadyMix™ (Sigma) qPCR kit. The primers used for the ChIP assay are listed in Supplementary Material, Table S1. The PCR program was: 94°C, 2 m; 39 cycles: 94°C, 40 s/ 59°C, 40 s/ 72°C, 40 s and Plate read; 75°C, 1 s/ 80°C, 1 s/ 82°C, 1 s. The immunoprecipitated DNA was normalized to the amount of H3. ChIP experiments were performed in duplicate for each biological sample, and each PCR was done in duplicate.

RNA high-throughput sequencing experiment

A standard Trizol (Invitrogen) protocol was used for total RNA extraction. The RNA quality was checked by Bioanalyzer RNA 6000 Nano (Agilent). RNA with a score >8 was used for preparing RNA-seq library using a TruSeq RNA Sample Prep v2 kit (Illumina). For the RNA sequencing analysis, raw reads were aligned to the human genome (hg19) using a Tophat aligner (57). Differential expression analysis was performed with DESeq Bioconductor package (58). GO ontology and Reactome pathway analysis was done on the genes found to be differentially expressed to test for enrichment of GO terms and pathways in the Reactome pathway database. Bioconductor package GOseq was used for this enrichment analysis. The package corrects for length bias present in RNASeq data (40). Raw *P*-values were adjusted for multiple testing using the Benjamini–Hochberg procedure. All GO categories over-represented with adjusted *P*-value of <0.05 were obtained. The sequencing data have been submitted to Gene Expression Omnibus data repository with the accession number: GSE42960 (59). The trend towards normalization of the biomarkers was calculated using the difference in gene expression levels between healthy and FRDA previously determined by Coppola *et al*. (32). Thus, we compared this difference in biomarker expression with the fold change in gene expression obtained from our primary lymphocyte cultures before and after nicotinamide treatment (denoted as Nico versus UT log2 fold change in Supplementary Material, Fig. S3).

SUPPLEMENTARY MATERIAL

Supplementary Material is available at *HMG* online.

Conflict of Interest statement. None declared.

FUNDING

This work was supported in part by Imperial College London, the Medical Research Council (UK), Ataxia UK, the European Friedreich's Ataxia Consortium for Translational Studies (EU EFACTS), and the National Institute for Health Research (NIHR) Biomedical Research Centre based at Imperial College Healthcare NHS Trust at the Imperial College Clinical Research Facility, Hammersmith Hospital. The views expressed are those of the authors and not necessarily those of the NHS, the NIHR or the Department of Health.

REFERENCES

1. Campuzano, V., Montermini, L., Molto, M.D., Pianese, L., Cossee, M., Cavalcanti, F., Monros, E., Rodius, F., Duclos, F., Monticelli, A. *et al.* (1996) Friedreich's ataxia: autosomal recessive disease caused by an intronic GAA triplet repeat expansion. *Science*, **271**, 1423–1427.
2. Yoon, T. and Cowan, J.A. (2004) Frataxin-mediated iron delivery to ferrochelatase in the final step of heme biosynthesis. *J. Biol. Chem.*, **279**, 25943–25946.
3. Koeppen, A.H., Michael, S.C., Knutson, M.D., Haile, D.J., Qian, J., Levi, S., Santambrogio, P., Garrick, M.D. and Lamarche, J.B. (2007) The dentate nucleus in Friedreich's ataxia: the role of iron-responsive proteins. *Acta Neuropathol*, **114**, 163–173.
4. Punga, T. and Buhler, M. (2010) Long intronic GAA repeats causing Friedreich ataxia impede transcription elongation. *EMBO Mol. Med.*, **2**, 120–129.
5. Schulz, J.B., Boesch, S., Burk, K., Durr, A., Giunti, P., Mariotti, C., Pousset, F., Schols, L., Vankan, P. and Pandolfo, M. (2009) Diagnosis and treatment of Friedreich ataxia: a European perspective. *Nat. Rev. Neurol.*, **5**, 222–234.
6. Koeppen, A.H. (2011) Friedreich's ataxia: pathology, pathogenesis, and molecular genetics. *J. Neurol. Sci.*, **303**, 1–12.
7. Ohshima, K., Montermini, L., Wells, R.D. and Pandolfo, M. (1998) Inhibitory effects of expanded GAA.TTC triplet repeats from intron I of the Friedreich ataxia gene on transcription and replication *in vivo*. *J. Biol. Chem.*, **273**, 14588–14595.
8. Bidichandani, S.I., Ashizawa, T. and Patel, P.I. (1998) The GAA triplet-repeat expansion in Friedreich ataxia interferes with transcription and may be associated with an unusual DNA structure. *Am. J. Hum. Genet.*, **62**, 111–121.
9. Grabczyk, E., Mancuso, M. and Sammarco, M.C. (2007) A persistent RNA.DNA hybrid formed by transcription of the Friedreich ataxia triplet repeat in live bacteria, and by T7 RNAP *in vitro*. *Nucleic Acids Res.*, **35**, 5351–5359.
10. Saveliev, A., Everett, C., Sharpe, T., Webster, Z. and Festenstein, R. (2003) DNA triplet repeats mediate heterochromatin-protein-1-sensitive variegated gene silencing. *Nature*, **422**, 909–913.
11. Festenstein, R. (2006) Breaking the silence in Friedreich's ataxia. *Nat. Chem. Biol.*, **2**, 512–513.
12. Herman, D., Jenssen, K., Burnett, R., Soragni, E., Perlman, S.L. and Gottesfeld, J.M. (2006) Histone deacetylase inhibitors reverse gene silencing in Friedreich's ataxia. *Nat. Chem. Biol.*, **2**, 551–558.
13. Greene, E., Mahishi, L., Entezam, A., Kumari, D. and Usdin, K. (2007) Repeat-induced epigenetic changes in intron 1 of the frataxin gene and its consequences in Friedreich ataxia. *Nucleic Acids Res.*, **35**, 3383–3390.
14. Al-Mahdawi, S., Pinto, R.M., Ismail, O., Varshney, D., Lymperi, S., Sandi, C., Trabzuni, D. and Pook, M. (2008) The Friedreich ataxia GAA repeat expansion mutation induces comparable epigenetic changes in human and transgenic mouse brain and heart tissues. *Hum. Mol. Genet.*, **17**, 735–746.
15. Dillon, N. and Festenstein, R. (2002) Unravelling heterochromatin: competition between positive and negative factors regulates accessibility. *Trends Genet.*, **18**, 252–258.
16. Chou, C.J., Herman, D. and Gottesfeld, J.M. (2008) Pimelic diphenylamide 106 is a slow, tight-binding inhibitor of class I histone deacetylases. *J. Biol. Chem.*, **283**, 35402–35409.
17. Rai, M., Soragni, E., Jenssen, K., Burnett, R., Herman, D., Coppola, G., Geschwind, D.H., Gottesfeld, J.M. and Pandolfo, M. (2008) HDAC inhibitors correct frataxin deficiency in a Friedreich ataxia mouse model. *PLoS One*, **3**, e1958.
18. Rai, M., Soragni, E., Chou, C.J., Barnes, G., Jones, S., Rusche, J.R., Gottesfeld, J.M. and Pandolfo, M. (2010) Two new pimelic diphenylamide HDAC inhibitors induce sustained frataxin upregulation in cells from Friedreich's ataxia patients and in a mouse model. *PLoS One*, **5**, e8825.
19. Sandi, C., Pinto, R.M., Al-Mahdawi, S., Ezzatizadeh, V., Barnes, G., Jones, S., Rusche, J.R., Gottesfeld, J.M. and Pook, M.A. (2011) Prolonged treatment with pimelic o-aminobenzamide HDAC inhibitors ameliorates the disease phenotype of a Friedreich ataxia mouse model. *Neurobiol. Dis.*, **42**, 496–505.
20. Gui, C.Y., Ngo, L., Xu, W.S., Richon, V.M. and Marks, P.A. (2004) Histone deacetylase (HDAC) inhibitor activation of p21WAF1 involves changes in promoter-associated proteins, including HDAC1. *Proc. Natl Acad. Sci. U S A*, **101**, 1241–1246.
21. Bolden, J.E., Peart, M.J. and Johnstone, R.W. (2006) Anticancer activities of histone deacetylase inhibitors. *Nature reviews Drug discovery*, **5**, 769–784.
22. Gottlicher, M., Minucci, S., Zhu, P., Kramer, O.H., Schimpf, A., Giavara, S., Sleeman, J.P., Lo Coco, F., Nervi, C., Pelicci, P.G. *et al.* (2001) Valproic acid defines a novel class of HDAC inhibitors inducing differentiation of transformed cells. *The EMBO J*, **20**, 6969–6978.
23. Beal, M.F., Henshaw, D.R., Jenkins, B.G., Rosen, B.R. and Schulz, J.B. (1994) Coenzyme Q10 and nicotinamide block striatal lesions produced by the mitochondrial toxin malonate. *Annals of neurology*, **36**, 882–888.
24. Bitterman, K.J., Anderson, R.M., Cohen, H.Y., Latorre-Esteves, M. and Sinclair, D.A. (2002) Inhibition of silencing and accelerated aging by nicotinamide, a putative negative regulator of yeast sir2 and human SIRT1. *J Biol Chem*, **277**, 45099–45107.
25. Dittenhafer-Reed, K.E., Feldman, J.L. and Denu, J.M. (2011) Catalysis and mechanistic insights into sirtuin activation. *Chembiochem : a European journal of chemical biology*, **12**, 281–289.
26. Vaquero, A., Scher, M., Lee, D., Erdjument-Bromage, H., Tempst, P. and Reinberg, D. (2004) Human SirT1 interacts with histone H1 and promotes formation of facultative heterochromatin. *Mol Cell*, **16**, 93–105.
27. Vaquero, A., Scher, M., Erdjument-Bromage, H., Tempst, P., Serrano, L. and Reinberg, D. (2007) SIRT1 regulates the histone methyl-transferase SUV39H1 during heterochromatin formation. *Nature*, **450**, 440–444.
28. Hagege, H., Klous, P., Braem, C., Splinter, E., Dekker, J., Cathala, G., de Laat, W. and Forne, T. (2007) Quantitative analysis of chromosome conformation capture assays (3C-qPCR). *Nat Protoc*, **2**, 1722–1733.
29. Simonis, M., Klous, P., Homminga, I., Galjaard, R.J., Rijkers, E.J., Grosveld, F., Meijerink, J.P. and de Laat, W. (2009) High-resolution identification of balanced and complex chromosomal rearrangements by 4C technology. *Nat Methods*, **6**, 837–842.
30. McArthur, M., Gerum, S. and Stamatoyannopoulos, G. (2001) Quantification of DNaseI-sensitivity by real-time PCR: quantitative analysis of DNaseI-hypersensitivity of the mouse beta-globin LCR. *J Mol Biol*, **313**, 27–34.
31. Nelson, J.D., Denisenko, O. and Bomsztyk, K. (2006) Protocol for the fast chromatin immunoprecipitation (ChIP) method. *Nat Protoc*, **1**, 179–185.
32. Coppola, G., Burnett, R., Perlman, S., Versano, R., Gao, F., Plasterer, H., Rai, M., Sacca, F., Filla, A., Lynch, D.R. *et al.* (2011) A gene expression phenotype in lymphocytes from Friedreich ataxia patients. *Annals of neurology*, **70**, 790–804.
33. Knip, M., Douek, I.F., Moore, W.P., Gillmor, H.A., McLean, A.E., Bingley, P.J. and Gale, E.A. (2000) Safety of high-dose nicotinamide: a review. *Diabetologia*, **43**, 1337–1345.
34. Kumari, D., Biacsi, R.E. and Usdin, K. (2011) Repeat expansion affects both transcription initiation and elongation in friedreich ataxia cells. *J Biol Chem*, **286**, 4209–4215.
35. Kim, E., Napierala, M. and Dent, S.Y. (2011) Hyperexpansion of GAA repeats affects post-initiation steps of FXN transcription in Friedreich's ataxia. *Nucleic Acids Res.*, **39**, 8366–8377.

36. De Biase, I., Chutake, Y.K., Rindler, P.M. and Bidichandani, S.I. (2009) Epigenetic silencing in Friedreich ataxia is associated with depletion of CTCF (CCCTC-binding factor) and antisense transcription. *PLoS One*, **4**, e7914.
37. Barski, A., Cuddapah, S., Cui, K., Roh, T.Y., Schones, D.E., Wang, Z., Wei, G., Chepelev, I. and Zhao, K. (2007) High-resolution profiling of histone methylations in the human genome. *Cell*, **129**, 823–837.
38. Rosenbloom, K.R., Sloan, C.A., Malladi, V.S., Dreszer, T.R., Learned, K., Kirkup, V.M., Wong, M.C., Maddren, M., Fang, R., Heitner, S.G. *et al.* (2012) ENCODE Data in the UCSC Genome Browser: year 5 update. *Nucleic Acids Res*., **41**, D56–D63.
39. Al-Mahdawi, S., Pinto, R.M., Ruddle, P., Carroll, C., Webster, Z. and Pook, M. (2004) GAA repeat instability in Friedreich ataxia YAC transgenic mice. *Genomics*, **84**, 301–310.
40. Young, M.D., Wakefield, M.J., Smyth, G.K. and Oshlack, A. (2010) Gene ontology analysis for RNA-seq: accounting for selection bias. *Genome Biol.*, **11**, R14.
41. Papaccio, G., Ammendola, E. and Pisanti, F.A. (1999) Nicotinamide decreases MHC class II but not MHC class I expression and increases intercellular adhesion molecule-1 structures in non-obese diabetic mouse pancreas. *J. Endocrinol.*, **160**, 389–400.
42. Kaneko, S., Wang, J., Kaneko, M., Yiu, G., Hurrell, J.M., Chitnis, T., Khoury, S.J. and He, Z. (2006) Protecting axonal degeneration by increasing nicotinamide adenine dinucleotide levels in experimental autoimmune encephalomyelitis models. *J. Neurosci.*, **26**, 9794–9804.
43. Gale, E.A., Bingley, P.J., Emmett, C.L. and Collier, T. (2004) European Nicotinamide Diabetes Intervention Trial (ENDIT): a randomised controlled trial of intervention before the onset of type 1 diabetes. *Lancet*, **363**, 925–931.
44. Hiromatsu, Y., Yang, D., Miyake, I., Koga, M., Kameo, J., Sato, M., Inoue, Y. and Nonaka, K. (1998) Nicotinamide decreases cytokine-induced activation of orbital fibroblasts from patients with thyroid-associated ophthalmopathy. *J. Clin. Endocrinol. Metab*, **83**, 121–124.
45. de Wit, E. and de Laat, W. (2012) A decade of 3C technologies: insights into nuclear organization. *Genes Dev.*, **26**, 11–24.
46. Elgin, S.C. (1996) Heterochromatin and gene regulation in Drosophila. *Curr. Opin. Genet. Dev.*, **6**, 193–202.
47. Sun, F.L., Cuaycong, M.H. and Elgin, S.C. (2001) Long-range nucleosome ordering is associated with gene silencing in Drosophila melanogaster pericentric heterochromatin. *Mol. Cell. Biol.*, **21**, 2867–2879.
48. Csink, A.K. and Henikoff, S. (1996) Genetic modification of heterochromatic association and nuclear organization in Drosophila. *Nature*, **381**, 529–531.
49. Canzio, D., Chang, E.Y., Shankar, S., Kuchenbecker, K.M., Simon, M.D. *et al.* (2011) Chromodomain-mediated oligomerization of HP1 suggests a nucleosome-bridging mechanism for heterochromatin assembly. *Mol. Cell*, **41**, 67–81.
50. Grewal, S.I. and Elgin, S.C. (2002) Heterochromatin: new possibilities for the inheritance of structure. *Curr. Opin. Genet. Dev.*, **12**, 178–187.
51. Pianese, L., Turano, M., Lo Casale, M.S., De Biase, I., Giacchetti, M., Monticelli, A., Criscuolo, C., Filla, A. and Cocozza, S. (2004) Real time PCR quantification of frataxin mRNA in the peripheral blood leucocytes of Friedreich ataxia patients and carriers. *J. Neurol. Neurosurg. Psychiatry*, **75**, 1061–1063.
52. Al-Mahdawi, S., Pinto, R.M., Varshney, D., Lawrence, L., Lowrie, M.B., Hughes, S., Webster, Z., Blake, J., Cooper, J.M., King, R. *et al.* (2006) GAA repeat expansion mutation mouse models of Friedreich ataxia exhibit oxidative stress leading to progressive neuronal and cardiac pathology. *Genomics*, **88**, 580–590.
53. Tolhuis, B., Palstra, R.J., Splinter, E., Grosveld, F. and de Laat, W. (2002) Looping and interaction between hypersensitive sites in the active beta-globin locus. *Mol. Cell.* **10**, 1453–1465.
54. Simonis, M., Klous, P., Splinter, E., Moshkin, Y., Willemsen, R., de Wit, E., van Steensel, B. and de Laat, W. (2006) Nuclear organization of active and inactive chromatin domains uncovered by chromosome conformation capture-on-chip (4C). *Nat. Genet.*, **38**, 1348–1354.
55. Thongjuea, S., Bergen Center for Computational Science and Norway (2011). r3Cseq: Analysis of Chromosome Conformation Capture and Next-generation Sequencing (3C-seq). R package version 1.4.0.
56. Teixe, T., Nieto-Blanco, P., Vilella, R., Engel, P., Reina, M. and Espel, E. (2008) Syndecan-2 and -4 expressed on activated primary human CD4+ lymphocytes can regulate T cell activation. *Mol. Immunol.*, **45**, 2905–2919.
57. Trapnell, C., Pachter, L. and Salzberg, S.L. (2009) TopHat: discovering splice junctions with RNA-Seq. *Bioinformatics*, **25**, 1105–1111.
58. Anders, S. and Huber, W. (2010) Differential expression analysis for sequence count data. *Genome Biol.*, **11**, R106.
59. Edgar, R., Domrachev, M. and Lash, A.E. (2002) Gene expression omnibus: NCBI gene expression and hybridization array data repository. *Nucleic Acids Res.*, **30**, 207–210.